CHEMISTRY OF MATERIALS

ARTICLE

pubs.acs.org/cm

Direct Formation of Thin-Walled Palladium Nanotubes in Nanochannels under an Electrical Potential

Lichun Liu[†] and Sungho Park*[,†,‡]

[†]Department of Chemistry, BK21 School of Chemical Materials Science, and [‡]SKKU Advanced Institute of Nanotechnology and Department of Energy Science, Sungkyunkwan University, Suwon 440-746, South Korea

Supporting Information

ABSTRACT: In this work, we demonstrate a simple methodology for synthesizing vertical or free-standing palladium (Pd) nanotube arrays in a highly efficient fashion. The hydroxyl-terminated surface of the nanochannel in an alumina membrane is used to form an interfacial double layer by specifically adsorbing hydrogen ions (H^+) from an acidic solution and leaving counterions to predominate in the diffuse layer. Locally enriched H^+ ions at the wall of alumina nanochannel produce a higher content of adsorbed hydrogen on the electrochemically reduced metallic Pd surface under an appropriate electric potential. The higher Pd growth rate at peripheral positions rather than elsewhere in the nanochannel was due to the dual reductions of Pd(II) compound by hydrogen and electric potential. The disparity of growth rates in combination with diffusion-controlled growth efficiently gives rise to the formation of nanotubes with wall thicknesses as narrow as 6 nm.

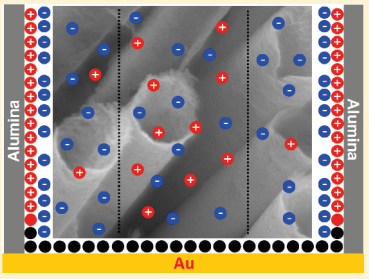

KEYWORDS: AAO, electrodeposition, double layer, hydrogen evolution, nanorod, nanotube, Palladium

INTRODUCTION

The construction of tubular nanostructures is an interesting topic in nanoscience due to the recognition of nanotubes as the true heirs to their solid counterparts in a variety of applications by virtue of their superior physical and chemical properties.[1] The high ratio of surface area to mass and the useful inner space of nanotubular materials meet the practical requirements of providing low cost, high efficiency, and versatility for applications.[2] Along with the abundance of research on carbon nanotubes, metallic nanotubes have also gained a share of the contemporary material science attention.[3] In particular, palladium (Pd), a member of the platinum group metals, has been valuable as a highly active catalyst in fuel cells,[4] organic synthesis,[5−7] and automobile exhaust converters; as a high-capacity absorber in hydrogen storage;[8] and as an extraordinarily sensitive material in hydrogen gas detection[9] for a long time. Until now, there have been several strategies available for the formation of Pd nanotubes including electrodeposition,[10,11] electroless deposition,[12,13] galvanic replacement,[14,15] the Kirkendall effect,[1] and molecular adsorption.[8] Yet more efficient methodologies for synthesizing superior Pd nanotubes are worthy of further exploration. Vertical nanotubes with thin walls would be ideal for maximizing the usage of Pd per unit mass, due principally to the large population of exposed surface atoms on both the inner and outer surfaces of standing walls and the ready accessibility to active sites at moderate-diameter open tubes for either gases or liquids. Compared to the commonly used template-directed, one-dimensional Pd nanowire[16−18] synthesis, nanotube structure formation via a hard-template method remains a challenge on account of the perceptible difficulty of forming a flimsy Pd film only on the inner wall without fully filling the void space of the nanochannels in a template. Herein, relying on the superficial chemical nature and geometrical configuration of an anodic aluminum oxide (AAO, a form of alumina with highly ordered nanochannels; Figure S1, Supporting Information) membrane template,[19] we were able to successfully synthesize a vertical thin-walled Pd nanotube array by regulating the interfacial double layer and the electric potential of hydrogen evolution.

EXPERIMENTAL SECTION

Materials. All chemicals were purchased from Sigma−Aldrich and used as received if not stated otherwise, and all aqueous solutions were prepared with triply distilled deionized water (Millipore, >18.2 MΩ). Au plating solution (Orotemp 24 RTU) was purchased from Technic Inc. Alumina membranes (AAO, diameter ≈13 mm, nanochannel diameter ≈300 nm, thickness ≈60 μm) were purchased from Whatman International Ltd. Homemade AAO was synthesized by the method described in our previous publication.[20]

Instruments. We performed all electrochemical experiments on an Autolab (PGSTAT12) equipped with a three-electrode system [counterelectrode, Pt mesh; reference electrode, Ag/AgCl (3 M KCl)]. We acquired SEM images on a JEOL JSM-7401F field emission scanning electron microscope (FE-SEM) and TEM images on a JEOL JEM2100F high resolution transmission electron microscope (HR-TEM).

Methods. Before AAO was used, an Au nanoparticles immobilized layer[21] on commercial AAO and a thermally evaporated Au film on homemade AAO were used as conducting layers. For TEM analysis, the free-standing Pd nanotubes were obtained by selectively dissolving Au

Received: October 20, 2010
Revised: December 20, 2010
Published: February 22, 2011

conducting layer by an aqueous gold etching solution consisting of 0.6 M KI and 0.2 M I_2 and following complete removal of alumina membrane by 3 M NaOH for 20 min and multiple rinse by deionized water. The solution in cell was degassed with N_2 for 20 min to remove O_2 before CO stripping experiments. During CO gas bubbling, the potential was kept at 0.3 V to avoid H_2 evolution.

RESULTS AND DISCUSSION

When an acidic solution is cast onto an AAO membrane, hydrogen ions (H^+) are adsorbed specifically onto the surface of the alumina, leading to the formation of interfacial double layers. It is well-known that the surfaces of most substances are electrically charged when contacted with a polar (e.g., aqueous) medium. A monolayer of Peri-modeled[22,23] hydroxyl groups (−OH) on the alumina surface has been characterized previously by observing the −OH bond stretching frequencies from infrared spectroscopic analysis. At a solution pH below the point of zero charge (PZC, ∼8−9), those −OHs on the alumina surface are ionized to produce a monolayer of positively charged $-OH_2^+$ groups[24,25] whose quantity mainly depends on the pH of the solution. Accordingly, the positively charged surface leads to the formation of an interfacial double layer at the solid−liquid interface by electrostatic interactions between $-OH_2^+$ on the alumina surface and negative ions present in bulk solution. The interfacial double layer exhibits significant features that determine the distribution of a nanometer-scale thin layer of either anions or cations near the solid surface. When the classical Gouy−Chapman−Stern's double layer model is taken into consideration, a plane distribution of ions at a solid−liquid interface is shaped on a flat surface. However, the distribution of a double layer along a porous surface differs from that at a flat surface and heavily relies on the ionic strength. The reciprocal relationship between double layer thickness and ionic strength of a solution has been extensively studied by electrochemists.[26]

In this original investigation, we used an aqueous solution containing 0.05 M $PdCl_2$ and 0.1 M HCl as a plating solution. Under the experimental conditions, H^+ ions do not coordinate with Pd ions because Pd(II) is a d-transition metal ion with vacant d orbitals that is apt to accept electron pairs from electron-donating ligands (Lewis base), such as Cl^- ions. The solubility of $PdCl_2$ (insoluble in water but particularly soluble in coordinating solvents) has been investigated by theoretical coordination considerations.[27] In addition, an experimental investigation of Droll et al.[28] has shown that Pd exists only as $PdCl_2$, $PdCl_3^-$, and $PdCl_4^{2-}$ in solution when the ratio of [Cl]/[Pd] is between 4.0 and 4.8. The resulting exclusive presence of cation and simple ionic components [H^+, Cl^- (excess), $PdCl_n^{(n-2)-}$ ($2 \le n \le 4$)] in the system facilitates the formation of a thick double layer. In this context, the double layer thickness in the alumina nanochannel can be flexibly tailored through control of the concentration of HCl (H^+) and the ratio of [Cl]/[Pd], although the exact measurement of double layer thickness is technically unavailable on such insulating and porous material.

In a nanochannel, Pd(II)−Cl complexes and a portion of free Cl^- ions reside in the negatively charged region, composed of a compact layer and a diffuse layer, whose magnitude of negative charge is equivalent to that of the opposite charge in the Stern layer[29] to maintain electroneutrality (Figure 1). Large numbers of H^+ from the acidic solution at low pH (e.g., pH = 1) far from the PZC of alumina are stabilized at the solid surface due to the high density of electronegative hydroxyl groups on the alumina

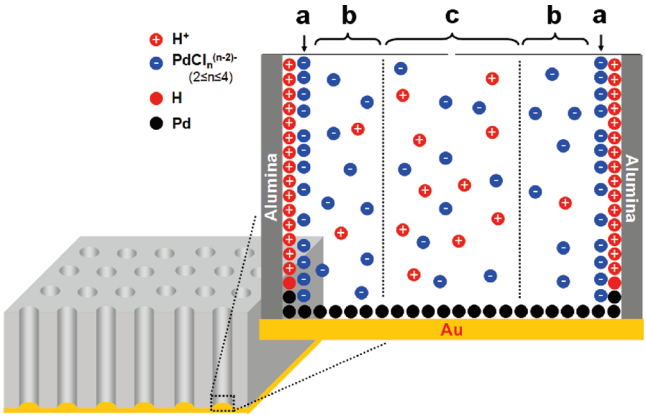

Figure 1. Schematic representation of the Gouy−Chapman−Stern modeled distribution of ions in a cross-sectional nanochannel and initial formation mechanism of vertical Pd nanotubes array (notice the compositions at the corners). a, b, and c correspond to compact layer, diffuse layer, and bulk solution regions in a nanochannel, respectively.

surface (5−20 $-OH/nm^2$).[22] The content of adsorbed H^+ on the inner wall of the nanochannel and the concentration of Pd(II)−Cl complexes in the compact layer are distinctly higher than in the bulk region, if it is supposed that the Donnan exclusion effect does not occur.[30,31] Upon application of a proper electric reduction potential, H^+ ions and Pd(II)−Cl complexes can be reduced simultaneously at the smooth Au bottom substrate (Figure 2A) in the initial stage, generating a thin layer of Pd aggregates with a rough morphology (Figure 2B). It occurs because H^+ ions and Pd(II)−Cl complexes are physically adsorbed on and diffuse to the Au substrate during solution filling and electric potential. As Pd atoms start to grow on the Au substrate, the hydrogen evolution reaction (HER), a widely investigated electrode reaction in electrochemistry, occurs on the surface of the cathodic Pd according to the well-accepted Volmer−Heyrovsky−Tafel reaction mechanism[32] in acidic conditions as follows.

$$M + H^+ + e \rightleftharpoons MH \text{ (Volmer)}$$

$$MH + H^+ + e \rightleftharpoons M + H_2 \text{ (Heyrovsky)}$$

$$2MH \rightleftharpoons 2M + H_2 \text{ (Tafel)}$$

where M denotes most transition metals.

Reduced hydrogen is readily adsorbed on atomic Pd through an exothermic process.[31,32] The generated hydrogen (either Volmer hydrogen atoms or Heyrovsky and Tafel hydrogen molecules) is a moderate reductant[33,34] with a standard reduction potential of 0 V (vs standard hydrogen electrode, SHE) which can reduce many high-valent metallic compounds, such as Pd(II)[35] with a standard reduction potential of 0.83 V[14] (vs SHE). We performed an additional experiment to show that gaseous hydrogen could reduce the Pd(II)−Cl complex in acidic solution, which was confirmed by the observation of a quick and noticeable color transition from bright yellow to dark black when hydrogen gas was introduced into the solution (Figure 3 panels A and B, before and after H_2 gas bubbling). Therefore, it is reasonable to conclude that chemically adsorbed hydrogen atoms on the electrochemically reduced Pd metal surface can more easily reduce Pd−Cl complex ions because they are more reactive than gaseous hydrogen molecules.

dx.doi.org/10.1021/cm103013z |Chem. Mater. 2011, 23, 1456–1460

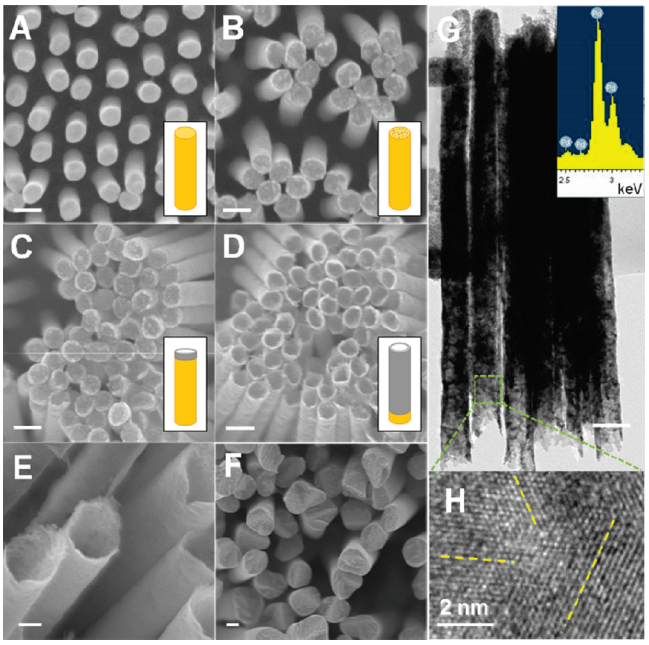

Figure 2. FE-SEM images of each step for Pd nanotube formation in AAO templates (pore $d \sim 80$ nm): (A) smooth top of Au nanorod; (B) roughened top of nanorod after deposition of a small amount of Pd, 10 mC/cm^2; (C) wall height grows faster than central positions observed after deposition of a little more Pd, 20 mC/cm^2; and (D) longer Pd nanotube obtained from more deposition of Pd, 0.2 C/cm^2. (E) Pd nanotubes at −0.1 V with commercial AAO (pore $d \sim 300$ nm). (F) SEM image of solid Pd nanorods formed at 0.3 V as compared to nanotubes shown in panel E. (G) TEM image of freestanding Pd nanotubes dissociated from sample in panel D. (Inset) EDAX, confirming pure Pd. (H) High-resolution TEM image showing multicrystalline Pd nanotubes. Scale bars in all images, 100 nm.

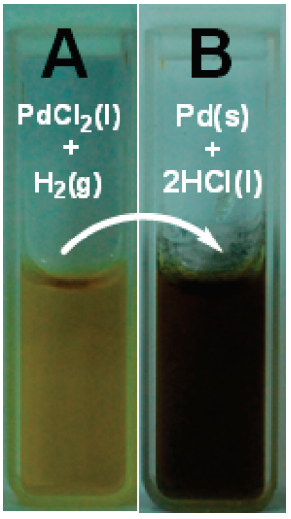

Figure 3. (A) Color of 10 mM $PdCl_2$ in 100 mM HCl. (B) Color of solution described in panel A after hydrogen gas bubbling for 2 min under 0.1 MPa pressure with silicone oil buffering.

The key to forming a tubular structure in a nanochannel is to induce a higher growth rate of the target material at peripheral positions rather than elsewhere. In this respect, it is essential to point out the particular role of the interfacial double layer and hydrogen evolution in leading to the formation of Pd nanotubes. The inner wall of the nanochannel is responsible for a higher local content of H^+ ions. Thus, more hydrogen should be generated at peripheral positions upon application of an appropriate electric potential. This induced difference of hydrogen concentration along the transverse section of the nanochannel leads to a large disparity of Pd growth rates between the peripheral positions and other places and therefore efficiently establishes the formation of a tubular structure after a very small amount of Pd deposition (Figure 2C). When the height of Pd at a peripheral position is somewhat higher than elsewhere, a depleted region on the Pd cathode is formed that leads to Pd(II)−Cl complexes diffusing to the elevated positions (tube wall) and not to other places. This process is reminiscent of the well-studied diffusion-controlled growth.[3] As indicated by Figure 2D, longer nanotubes with 6 nm thick walls were regularly synthesized by continuously increasing the passed amount of charge. The hollow interior and polycrystallinity characteristics of the nanotubes can be observed in the TEM images in Figure 2, panels G and H, respectively. With respect to larger nanochannel sizes, we were also successful in preparing Pd nanotube structures using AAO membranes with pore $d \sim 300$ nm (Figure 2E).

In order to better understand the requisite roles of hydrogen and the double layer on nanotube formation, we performed a series of control experiments. First, hydrogen evolution was suppressed by tuning the electric potential out of the region where hydrogen evolution occurs. As expected, solid Pd nanorods, rather than nanotubes, were formed at electric potentials from 0.1 to 0.3 V (Figure 2F for AAO with pore $d \sim 300$ nm and Figure S2, Supporting Information, for AAO with pore $d \sim 80$ nm). The current levels at −0.1 and 0.3 V, for instance, are on the same order of magnitude (Figure S3, Supporting Information). This feature rules out the current level induced nanotube formation mechanism reported by Yoo and Lee,[11] who manipulated the current density by more than 2 orders of magnitude to transform nanorods at 0.1−1 mA/cm^2 to nanotubes at 200 mA/cm^2. In another experiment to probe H^+ ion involvement, the nanotube structure did not form under basic conditions where ammonia−water was used instead of acid. On the other hand, the double layer thickness decreased as the ionic strength of the solution was increased. At higher concentrations of HCl (e.g., 400 mM), the generation of solid nanorod structures arises from a double layer in the nanochannel that is too thin and indiscriminate concentrations of H^+ ions across the transverse section (Figure S4, Supporting Information). In contrast, Pd nanotubes formed well with lower concentrations of HCl ranging from 10 to 150 mM (the concentration of $PdCl_2$ was fixed at 10 mM).

We conducted a CO oxidation experiment to demonstrate the superiority of Pd nanotubes over nanorods with respect to electrocatalytic activity, relative effective surface area, and hydrogen storage capacity. The total area of hydrogen desorption peaks was about 2 times larger from Pd nanotubes than from nanorods (Figure 4A). The hydrogen storage capacity also improved with the nanoscale tubular structure. With the most important practical issue on the usage of these materials, we found that a 10-fold enhanced effective surface area per unit mass was achieved with Pd nanotubes as compared to nanorods of the same diameter.

Carbon monoxide (CO) is produced as an intermediate in the oxidation of many small organic molecules and is easily chemisorbed on the electrocatalytically active surface of metals such as

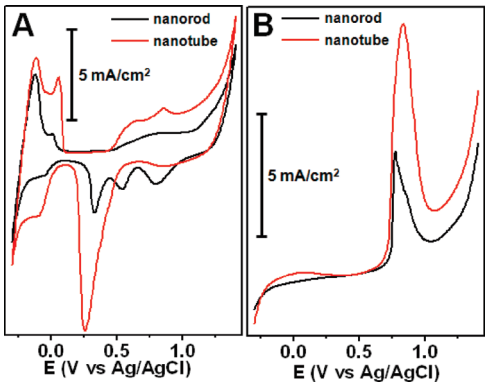

Figure 4. (A) Cyclic voltammetry of as-prepared Pd nanotubes (red trace) and nanorods (black trace). (B) Anodic stripping of irreversibly adsorbed CO molecules on Pd nanotubes (red trace) and nanorods (black trace). H_2SO_4 (0.1 M) was used as electrolyte in all CV studies. Scan rate, 20 mV/s.

Pd. A monolayer of chemisorbed CO molecules was artificially formed on the effective surface of our Pd nanostructures by bubbling CO gas into the solution (details shown in Supporting Information). The CO monolayer coverage prevented the Pd surface from adsorbing hydrogen, as was revealed by anodic scanning where the hydrogen desorption peak around −0.15 to 0 V was not observed in the first cycle and appeared in the second cycle after oxidation of CO (Figure 4B; only the first scan is shown for clarity). The onset potentials of anodic CO on Pd nanotubes and nanorods were similar at 0.7 V. The small peak delay and peak tailing of anodic stripping of CO from Pd nanotubes in Figure 4B demonstrate the slow kinetics of the oxidation reaction as compared to Pd nanorods. A shift of Pd oxide reduction peak from 0.30 V for nanorods to 0.23 V (vs Ag/AgCl) for nanotubes correlates to the formation of a stronger oxide bond (Pd−O and Pd−OH).[36] From mathematical integration, the peak area of CO oxidation on Pd nanotubes was approximately twice that of a similar length of Pd nanorods, indicating the nanotube has two exposed surfaces (an outer and an inner surface). Moreover, the peaks near 0 V suggest the weaker (left) and stronger (right) adsorption of hydrogen.

CONCLUSIONS

In conclusion, vertical thin-walled Pd nanotube arrays were readily fabricated with the assistance of alumina membranes by use of the synergistic effects of interfacial double layer formation and hydrogen evolution. As described in the main text, the key for direct formation of nanotubes is related to the appropriate reduction potential. The total length of nanotubes is limited by the AAO nanochannel length. We could not observe the transition of nanotubes to nanorods at a certain point. The longest length we have tried is 5 μm. This synthetic methodology significantly highlighted the usefulness of template substance surfaces on constructing superior nanostructures without intricate treatments. The Pd nanotube arrays may be considered a general secondary template to direct the formation of other nanotube structures. More importantly, the fundamental principles of Pd nanotube formation discerned from this study can be used to explore versatile extensions of Pd nanotube structures with alumina scaffolds.

ASSOCIATED CONTENT

Supporting Information. Four figures, showing SEM images of a typical homemade AAO template and Pd nanorods and a comparison of current levels between −0.1 V (for Pd nanotube) and +0.3 V (for Pd nanorod). This material is available free of charge via the Internet at http://pubs.acs.org.

AUTHOR INFORMATION

Corresponding Author

*E-mail spark72@skku.edu; fax 82-31-290-7075.

ACKNOWLEDGMENT

This work was supported by the National Research Foundation of Korea [World Class University (WCU) R31-2008-10029, Nano R&D program 2010-0019149 and 2010-0015457, and Priority Research Centers Program NRF-20090094025].

REFERENCES

(1) Fan, H. J.; Gösele, U.; Zacharias, M. *Small* **2007**, *3* (10), 1660–1671.
(2) Liu, L.; Yoo, S.-H.; Park, S. *Chem. Mater.* **2010**, *22* (8), 2681–2684.
(3) Lee, W.; Scholz, R.; Nielsch, K.; Gösele, U. *Angew. Chem.* **2005**, *117* (37), 6204–6208.
(4) Mazumder, V.; Sun, S. *J. Am. Chem. Soc.* **2009**, *131* (13), 4588–4589.
(5) Niwa, S.-i.; Eswaramoorthy, M.; Nair, J.; Raj, A.; Itoh, N.; Shoji, H.; Namba, T.; Mizukami, F. *Science* **2002**, *295* (5552), 105–107.
(6) Amatore, C.; Jutand, A. *Acc. Chem. Res.* **2000**, *33* (5), 314–321.
(7) Kim, S.-W.; Kim, M.; Lee, W. Y.; Hyeon, T. *J. Am. Chem. Soc.* **2002**, *124* (26), 7642–7643.
(8) Steinhart, M.; Jia, Z.; Schaper, A. K.; Wehrspohn, R. B.; Gösele, U.; Wendorff, J. H. *Adv. Mater.* **2003**, *15* (9), 706–709.
(9) Favier, F.; Walter, E. C.; Zach, M. P.; Benter, T.; Penner, R. M. *Science* **2001**, *293* (5538), 2227–2231.
(10) Cherevko, S.; Fu, J.; Kulyk, N.; Cho, S. M.; Haam, S.; Chung, C. H. *J. Nanosci. Nanotechnol.* **2009**, *9* (5), 3154–3159.
(11) Yoo, W. C.; Lee, J. K. *Adv. Mater.* **2004**, *16* (13), 1097–1101.
(12) Yu, S.; Welp, U.; Hua, L. Z.; Rydh, A.; Kwok, W. K.; Wang, H. H. *Chem. Mater.* **2005**, *17* (13), 3445–3450.
(13) Chu, S. Z.; Kawamura, H.; Mori, M. *J. Electrochem. Soc.* **2008**, *155* (5), D414–D418.
(14) Sun, Y.; Mayers, B. T.; Xia, Y. *Nano Lett.* **2002**, *2* (5), 481–485.
(15) Hermann, A. M.; Ramakrishnan, P. A.; Badri, V.; Mardilovich, P.; Landuyt, W. *Int. J. Hydrogen Energy* **2001**, *26* (12), 1295–1299.
(16) TaşAltin, N.; Öztürk, S.; Kilinç, N.; Yüzer, H.; Öztürk, Z. Z. *Nanoscale Res. Lett.* **2010**, 1–7.
(17) Kartopu, G.; Habouti, S.; Es-Souni, M. *Mater. Chem. Phys.* **2008**, *107* (2−3), 226–230.
(18) Wang, H.; Xu, C.; Cheng, F.; Jiang, S. *Electrochem. Commun.* **2007**, *9* (5), 1212–1216.
(19) Martin, C. R. *Science* **1994**, *266* (5193), 1961–1966.
(20) Kim, S.; Shuford, K. L.; Bok, H. M.; Kim, S. K.; Park, S. *Nano Lett.* **2008**, *8* (3), 800–804.
(21) Yoo, S.-H.; Liu, L.; Park, S. *J. Colloid Interface Sci.* **2009**, *339* (1), 183–186.
(22) Kasprzyk-Hordern, B. *Adv. Colloid Interface Sci.* **2004**, *110* (1−2), 19–48.
(23) Alexander, M. R.; Beamson, G.; Bailey, P.; Noakes, T. C. Q.; Skeldon, P.; Thompson, G. E. *Surf. Interface Anal.* **2003**, *35* (8), 649–657.
(24) Sprycha, R. *J. Colloid Interface Sci.* **1989**, *127* (1), 1–11.
(25) Regalbuto, J. R.; Navada, A.; Shadid, S.; Bricker, M. L.; Chen, Q. *J. Catal.* **1999**, *184* (2), 335–348.

(26) Boo, H.; Park, S.; Ku, B. Y.; Kim, Y.; Park, J. H.; Kim, H. C.; Chung, T. D. *J. Am. Chem. Soc.* **2004**, *126* (14), 4524–4525.
(27) Riebling, E. F. *Science* **1968**, *162* (3852), 467–468.
(28) Droll, H. A.; Block, B. P.; Fernelius, W. C. *J. Phys. Chem.* **1957**, *61* (7), 1000–1004.
(29) Das, S.; Chakraborty, S. *Langmuir* **2010**, *26* (13), 11589–11596.
(30) Schoch, R. B.; Han, J.; Renaud, P. *Rev. Mod. Phys.* **2008**, *80* (3), 839.
(31) Bluhm, E. A.; Bauer, E.; Chamberlin, R. M.; Abney, K. D.; Young, J. S.; Jarvinen, G. D. *Langmuir* **1999**, *15* (25), 8668–8672.
(32) Lipkowski, J.; Ross, P. N., *Electrocatalysis*: Wiley−VCH, Inc., New York, 1998.
(33) Luidold, S.; Antrekowitsch, H. *JOM* **2007**, *59* (6), 20–26.
(34) Luidold, S.; Antrekowitsch, H. *JOM* **2007**, *59* (10), 58–62.
(35) Henglein, A. *J. Phys. Chem. B* **2000**, *104* (29), 6683–6685.
(36) Yoo, S. H.; Park, S. *Adv. Mater.* **2007**, *19* (12), 1612–1615.